PAPER

Check for updates

Improved lithium-ion battery cathode rate performance *via* carbon black functionalization†

Donghyuck Park, [ID] [a] Peter C. Sherrell, [ID] [ab] Fangxi Xie[ac] and Amanda V. Ellis [ID] *[a]

Carbon black (CB) creates essential electron transport pathways in lithium-ion battery (LiB) cathodes. Here, we show that by modifying the surface of CB *via* mild hydrogen peroxide or nitric acid treatment, the rate performance of a LiB cathode can be increased up to 350% at 0.75 C-rate charging. We demonstrate that this improvement is predominantly due to the presence of introduced carbonyl groups on the surface of the CB which increases the surface redox reaction of the nickel manganese cobalt oxide (NMC) cathode active material. As a result, there is both a decrease in the overpotential (∼37% during 0.25 C-rate charging) and electrochemical impedance. A mechanism is proposed which describes how the cathode performance is influenced by electrostatic interactions between the CB surface and solvated lithium ions. An improved rate effect was demonstrated across various cathode active materials, clearly highlighting the versatility of this simple approach.

1. Introduction

Lithium-ion batteries (LiBs), as a bridge towards a green energy transformation, have a rapidly expanding role in society, ranging from powering personal electronics,[1] to hybrid or fully electric vehicles,[2–4] as well as managing intermittent power supply from renewable energy on the national grid.[5,6] Amongst the components within LiBs, the cathode plays a critical role in the cell-level performance metrics such as accessible capacity and rate performance.[7–9] The most commonly researched cathode is nickel manganese cobalt oxide (NMC), with an electrical resistance of $\sim 10^{-7}$ to $\sim 10^{-2}$ S m^{-1}.[10] Most LIB research has focused on the active material including its chemistry,[8,11] coating,[12] cathode–electrolyte interface,[13–15] and electrode design.[16] In particular, focus has been on increasing the cathode capacity and rate performance by enhancing the Li$^+$ ion transport at the cathode–electrolyte interface.

In order to boost a cathodes electronic conductivity, carbon black (CB) is added as a conductive additive in the vast majority of LiBs.[17,18] In addition, CB aids in the formation of ionic

pathways for lithium-ion (Li$^+$) diffusion where the electrolyte fills the pores in the cathode.[19] In 2019, Park *et al.*[20] used conductive single-walled carbon nanotubes (SWCNTs) in high energy density LiBs, finding that the high aspect ratio, conductivity and mechanical strength of the SWCNTs provided exceptional performance, up to 29 mA h cm^{-2}. However, CB remains the conductive additive of choice in LiBs due to its simple synthesis and low cost. However, while the electronic properties of CBs are well understood, how CB influences ionic transport within the cathode requires further study.

One path to improve CBs ionic transport properties is *via* chemical functionalization of its surface. The chemical modification of CB, in general, has been studied extensively, particularly for the introduction of oxygen-containing functionalities onto its surface.[21] The majority of approaches have used strong chemical oxidizing agents such as sulfuric acid (H$_2$SO$_4$),[22–24] potassium permanganate (KMnO$_4$),[25,26] or high concentration nitric acid (>60% HNO$_3$),[27,28] all of which oxidize the target carbon material while simultaneously generating defects within the CB structure.

In LiB anodes, the role of defects and surface functionalities of the graphite active material has been well studied and shown to contribute to an increased Li$^+$ ion storage capacity and facilitate Li$^+$ ion diffusion.[29–33] In particular, oxygen groups have been shown to exhibit strong Li$^+$ ion absorption, leading to enhanced capacity and rate performance.[34] Furthermore, hydroxyl (–C–OH) and carboxyl (–COOH) groups on the graphite have potential to reduce the energy barrier of Li$^+$ ion intercalation by generating a chemical interaction with the electronegative oxygen atoms in the carbonate molecules within the electrolyte.[35] Despite these detailed studies on graphite anodes,

[a]Department of Chemical Engineering, The University of Melbourne, Grattan Street, Parkville, Victoria, 3010, Australia. E-mail: amanda.ellis@unimelb.edu.au

[b]School of Science, RMIT University, Melbourne, Victoria, 3001, Australia

[c]School of Chemical Engineering and Technology, Sun Yat-Sen University, Zhuhai, 519082, P. R. China

† Electronic supplementary information (ESI) available: Experimental information, XPS analysis, Raman spectroscopy analysis, SEM images, cyclic voltammograms at various scan rates, peak separation potential analysis, electrochemical stability test, distribution of relaxation times analysis details, contact angle measurements, rate performance and GCD curves analysis for various cathode materials, schematic diagram of chemical treatment, XRD analysis, note for electronic conductivity and percolation effect. See DOI: https://doi.org/10.1039/d3ta05093a

4884 | *J. Mater. Chem. A*, 2024, **12**, 4884–4892

This journal is © The Royal Society of Chemistry 2024

the role of oxygen-containing groups on CBs within a cathode have not been well explored.

In this work, the role of oxygen functional groups (hydroxyl, carbonyl (–C=O) and carboxyl) on CB, in LiB cathodes, is studied. Commercial CB, SuperP, was treated under various mild oxidation conditions. Raman spectroscopy and X-ray photoelectron spectroscopy (XPS) were used to show defect generation and oxygen surface functionalities, respectively. NMC cathodes doped with functionalized CBs were investigated for surface redox behaviour, electrical conductivity, rate performance and electrochemical impedances. Finally, the functionalized CB was applied with other cathode active materials, namely, $Ni_{0.8}Mn_{0.2}Co_{0.2}O_2$ (NMC811), lithium manganese oxide ($LiMn_2O_4$) (LMO), and nickel cobalt aluminium oxide ($Ni_{0.8}Co_{0.15}Al_{0.05}O_2$) (NCA) to evaluate the rate performances compare to pristine SuperP.

2. Results and discussion

2.1 Chemical modification of carbon black

Elucidating the role that CB plays in ion transport is critical to minimizing the rapid charging and discharging in LiBs. Modifying CB with various surface functional groups without sacrificing electronic conductivity will enable the study of such ion transport effects. To avoid the formation of a significant number of defects in the CB, and associated loss of electronic conductivity, mild oxidizing agents were used to enable control over surface functional group formation (Fig. 1a). To this end, CB was treated with H_2O_2 at 70 °C for 24, 48 or 72 h, as well as 20% v/v or 70% v/v HNO_3 for 1.5 h. Raman spectroscopy was performed on the pristine and modified CBs to measure defect generation. The Raman spectra of CB is dominated by the D-band ($\sim$1350 cm^{-1}, disordered phase, out-of-plane vibration attributed to the defects[36]) and the G-band ($\sim$1582 cm^{-1}, graphitic phase, in-plane vibration of sp^2 bonding[37]), with the I_D/I_G ratio is proportional to the degree of sp^3 defects.[38] Fig. 1b and c displays the I_D/I_G ratios for the H_2O_2- and HNO_3-treated CBs, respectively. The intensity of the I_D/I_G ratio for the H_2O_2-treated CBs (Fig. 1b) remained constant from over the course of 72 h treatment at 1.63 ± 0.03 (pristine) to 1.61 ± 0.10 (72 h), indicating minimal defect generation.[39,40] Mild HNO_3 (20% v/v) treated CB showed a similar defect level ($I_D/I_G = 1.60 \pm 0.19$) to both untreated CB (1.63 ± 0.03) and 72 h H_2O_2 (1.61 ± 0.10) treated CB (Fig. 1c). This lack of defect generation is important as it avoids changes in chemical and electrical properties arising from defects that can interfere with the evaluation of oxygen groups. However, stronger HNO_3 (70% v/v) treatment generated significant new defects ($I_D/I_G = 2.03 \pm 0.21$) (Fig. 1d).

Oxygen functionalization of the CBs was monitored using XPS (Fig. S1–S4†). XPS peaks in the O 1s region were fitted using CASA XPS software (see Fig. S3 and Table S1†). The peak centred at $\sim$533.0 eV was assigned to C–O bonding, which mainly corresponds to C–OH and/or COOH.[41] The peak centred at $\sim$531.5 eV was assigned to C=O bonding which mainly corresponds to –C=O or –COOH functional groups[42] (Fig. 1a). Peng et al.[39] and Vincente-Santiago et al.[40] have demonstrated that the atomic concentration ratios of the C–O to C=O can be used to
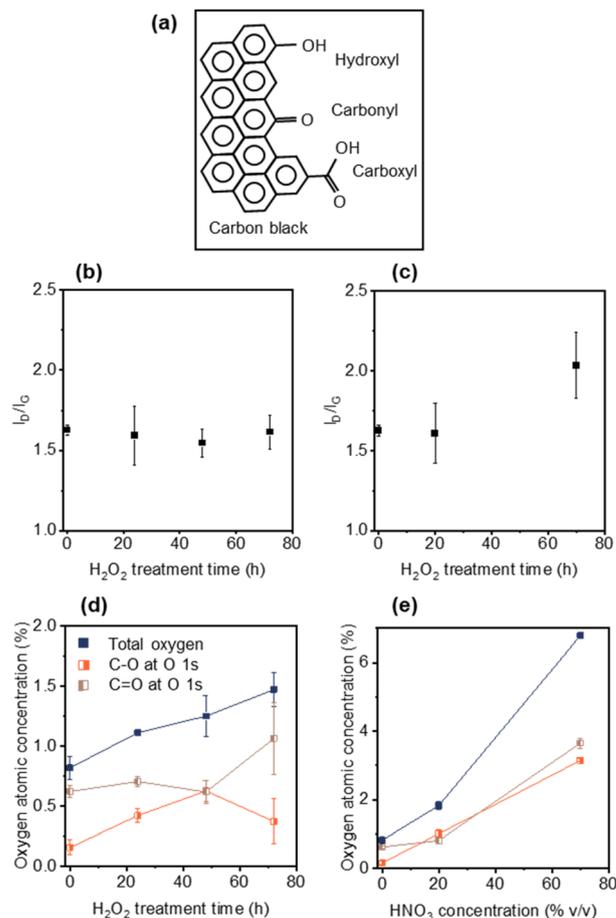

Fig. 1 (a) Schematic of oxygen-containing functional groups on CB, namely –C–OH (hydroxyl), –C=O (carbonyl) and –COOH (carboxyl). Oxygen atomic concentrations of analysed XPS spectra for (b) H_2O_2-treated CB for 0, 24, 48 and 72 h and (c) HNO_3-treated CB with 20% v/v and 70% v/v. Raman intensity ratios of D- to G-band (I_D/I_G) for (d) H_2O_2-treated CB for 0, 24, 48 and 72 h and (e) HNO_3-treated CB with 20% v/v and 70% v/v. The error bars represent standard error.

identify the dominant oxygen functional group species (C–OH, C=O, or COOH) on a carbon material.

Treatment with H_2O_2 for 24 h, 48 h and 72 h showed an increase in the minimal total oxygen content from 0.82 ± 0.09 at% (pristine) to 1.47 ± 0.14 at% (72 h) (Fig. 1d and Table 1). After 24 h H_2O_2 treatment the C–OH content appeared to dominate (noting that the C=O at% remains higher than the C–O at% due to the initial functional groups on pristine CB), with the C–O content increasing from 0.16 ± 0.06 at% to 0.42 ± 0.06 at%. From 24 h to 48 h the C–O content increased from 0.42 ± 0.06 at% to 0.63 ± 0.09 at% with a constant level of C=O. However, between 48 h and 72 h a marked change in C–O content was observed, decreasing from 0.63 ± 0.09 at% to 0.37 ± 0.19 at% with a corresponding increase in C=O content from 0.62 ± 0.10 at% to 1.07 ± 0.30 at%, resulting in C=O groups dominating the modified CB. The tendency of H_2O_2 treatment to preferentially oxidize C–OH groups to C=O groups, over generating new C–OH groups on the surface of CB, is in good agreement with reported literature.[39,40]

This journal is © The Royal Society of Chemistry 2024

J. Mater. Chem. A, 2024, **12**, 4884–4892 | **4885**

Table 1 Oxygen atomic concentration (calculated from XPS peak fitting) and Raman I_D/I_G ratios of chemically treated CB

| Treatment | Sample name | Atomic concentration (at%) | | | I_D/I_G |
		Total O	O 1s C–O	O 1s C=O	
Pristine	CB	0.82 ± 0.09	0.16 ± 0.06	0.62 ± 0.05	2.95 ± 0.10
H_2O_2 24 h	CB–OH (24 h)	1.11 ± 0.01	0.42 ± 0.06	0.71 ± 0.04	3.08 ± 0.15
H_2O_2 48 h	CB–OH (48 h)	1.25 ± 0.17	0.63 ± 0.09	0.62 ± 0.10	3.11 ± 0.20
H_2O_2 72 h	CB=O (72 h)	1.47 ± 0.14	0.37 ± 0.19	1.07 ± 0.30	3.24 ± 0.22
HNO_3 20% v/v	CB–COOH (20%)	1.83 ± 0.11	1.01 ± 0.11	0.81 ± 0.09	3.18 ± 0.27
HNO_3 70% v/v	CB–COOH (70%)	6.79 ± 0.10	3.15 ± 0.04	3.65 ± 0.14	3.69 ± 0.32

In contrast, for both 20% v/v and 70% v/v HNO_3 treatments both C–O and C=O content are shown to increase (Fig. 1e and Table 1), consistent with the reported literature for the formation of COOH groups via HNO_3 treatment (where $2CH_2 + 5HNO_3 \rightarrow 2COOH + 5HNO_2 + H_2O$).[24,28,39,43–45] The 20% v/v HNO_3 treated CB showed a higher oxygen content than H_2O_2 72 h CB (1.82 vs. 1.47 at%) despite similar defect levels. This result is explained by the tendency of HNO_3 treatment to form carboxyl-functional groups, which have 2 oxygen atoms per sp^3 defect site (compared to 1 : 1 for hydroxyl- or carbonyl- functional groups in Fig. 1a). Note that no nitrogen signal was observed in the XPS spectrum (Fig. S4†) and that epoxy groups (C–O–C bending at ~850 cm^{-2})[46] were not observed in any of the Raman spectra (Fig. S5†).

Thus, from here on each sample is denoted by its oxygen-functionality dominance, as CB; CB–OH (24 h); CB–OH (48 h); CB=O (72 h); CB–COOH (20%); and CB–COOH (70%).

2.2 Electrochemical characterisation

2.2.1 Cyclic voltammetry and galvanostatic charge/discharge.
To evaluate the role of the different CB oxygen-containing functional groups on the electrochemical reaction of a LiB cathode, a composite cathode was made using $LiNi_{0.6}Mn_{0.2}Co_{0.2}O_2$ (NMC622, the commercial standard cathode active material). Here, 5 wt% of pristine or modified CB was added as the conductive additive (Fig. 2a and S6†). 5 wt% is the standard concentration of CB added in commercial cathodes.[47–49] Due to the generation of a significant number of new defects which prevent deconvolution of surface modification and electronic effects, CB–COOH (70%) was not evaluated electrochemically. As such CB–COOH (70%) was not studied further in this work.

The electrochemical performance of the pristine and modified CBs was investigated using cyclic voltammetry (CV) at a scan rate of 0.1 mV s^{-1} (Fig. 2b). In the CV, the anodic peak corresponds to Li$^+$ ion de-insertion, and the anodic peak corresponds to Li$^+$ ion insertion. The data shows an increase in anodic and cathodic peaks in the order of: CB=O (72 h) 0.138 A g^{-1}, -0.104 A g^{-1} > CB–OH (48 h) 0.135 A g^{-1}, -0.103 A g^{-1} > CB–OH (24 h) 0.133 A g^{-1}, -0.102 A g^{-1} > CB 0.129 A g^{-1}, -0.096 A g^{-1} > CB–COOH (20%) 0.122 A g^{-1}, -0.092 A g^{-1}. The largest current peaks for CB=O (72 h) indicate that this cathode has the fastest reaction rate of deintercalation and intercalation of Li$^+$ ions. According to the

Nernst equation, the gap between the specific voltages at which the anodic and cathodic peaks appear, is inversely proportional to the electron transfer rate. Thus, as CB=O (72 h) has the lowest peak separation potential (Table S1†) as it undergoes the most efficient electrochemical reaction for charging/discharging compared to the other cathodes.

CVs at various scan rates (0.1, 0.2, 0.3, 0.4, 0.5, 0.6, 0.8, 1.0, 1.2 and 1.5 mV s^{-1}) were performed on the CB, CB–OH (24 h), CB–OH (48 h), CB=O (72 h), and CB–COOH (20%) cathodes (Fig. S7†). The current response could be distinguished into faradaic current (i_F) and non-faradaic electrochemical double-layer current (EDLC), with i_F arising from both the surface redox reaction at the electrode–electrolyte interface (i_S) and bulk
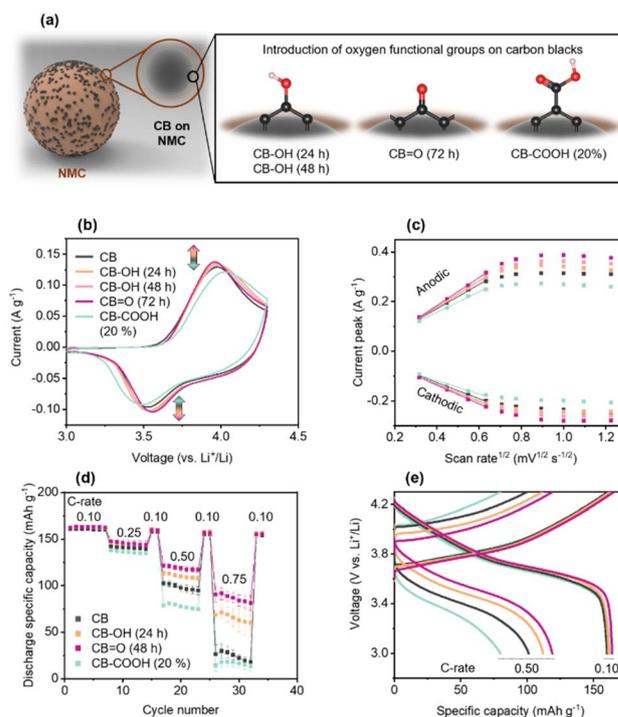

Fig. 2 Electrochemical tests for NMC622 cathodes fabricated using modified CBs. (a) Schematic of oxygen-containing functional groups on CB. (b) CV with a scan rate of 0.1 mV s^{-1}. (c) Anodic and cathodic current peaks at a scan rate of 0.1–1.5 mV s^{-1} versus the square root of the scan rate (mV$^{1/2}$ s$^{-1/2}$), a linear interval of 0.1–0.4 mV s^{-1} was fitted. (d) Rate performance of the NMC622 cathodes at 0.10, 0.25, 0.50, and 0.75 C-rates, error bars represent standard deviations. (e) GCD curves at 0.1 and 0.5 C-rates.

4886 | J. Mater. Chem. A, 2024, **12**, 4884–4892

This journal is © The Royal Society of Chemistry 2024

diffusion reactions (i_B) on the cathode material.[50,51] Note, that the current originating from the EDLC is commonly ignored because of its small overall contribution;[52] thus i_F can be derived from the Randles–Sevcik equation, eqn (1).[53,54]

$$i_F = i_S + i_B = k_1 v + k_2 v^{1/2} \tag{1}$$

Here, k_1 and k_2 correspond to surface reactions and diffusion reactions which are proportional to the applied scan rate v and $v^{1/2}$, respectively. For analytical purposes, the current peak (A g^{-1}) *versus* the square root of the scan rate ($mV^{1/2}$ $s^{-1/2}$) is shown in Fig. 2c and tabulated in Table S2.† As the scan rate increases, the amplitude of the current peaks linearly increases with the square root of the scan rate from 0.1 to 0.4 mV s^{-1} (Fig. 2c). At higher scan rates (above 0.8 mV s^{-1}) the current plateaus, reaching saturation as the Li$^+$ ions undergoing electrochemical reactions are decreased. The linear fitted slope (Fig. 2c) represents the surface redox reaction, with steeper slopes representing faster surface redox reactions. The results show that CB–OH (24 h) (anodic slope: 0.52), CB–OH (48 h) (anodic slope: 0.53) and CB=O (72 h) (anodic slope: 0.57) have advantageous (faster) surface redox reactions compared to pristine CB in both the anodic and cathodic reactions. In contrast, the lower slopes of the CB–COOH (20%) (anodic slope: 0.42) indicate that the surface redox reaction is hindered by COOH groups. The same trends were observed in the peak separation potential analysis (Fig. S8 and Table S5†).

The practical performance of the cathodes was evaluated *via* GCD in the voltage range of 3.0–4.3 V *vs.* Li$^+$/Li, as shown in Fig. 2d and e. The potential window of 3.0–4.3 V *vs.* Li$^+$/Li was chosen as standard cut-off voltage of NMC cathode.[55–57] All samples showed similar GCD curves, delivering a discharge capacity of ~160 mA h g^{-1} at 0.10C (C-rate is calculated based on the theoretical capacity of ~277.4 mA h g^{-1}). NMC622 typically has an accessibly capacity of 158–174 mA h g^{-1} at 0.10C depending on the active material mass loading and electrode structure.[58]

As the C-rate is increased to 0.10, 0.25, 0.50, and 0.75C, differences in the cathode rate performance of NMC622 cathodes made with modified CBs are observed. The pristine CB cathode showed a significant decrease in capacity at 0.75C down to 24.4 mA h g^{-1}, around 15% of the capacity at 0.10C. Similarly, the CB–COOH (20%) cathode showed a lower performance at 16.1 mA h g^{-1} at 0.75C. However, both CB–OH (24 h) and CB=O (72 h) cathodes showed a dramatically improved performance at 0.75C, at 65.4 mA h g^{-1} and 86.5 mA h g^{-1}, respectively.
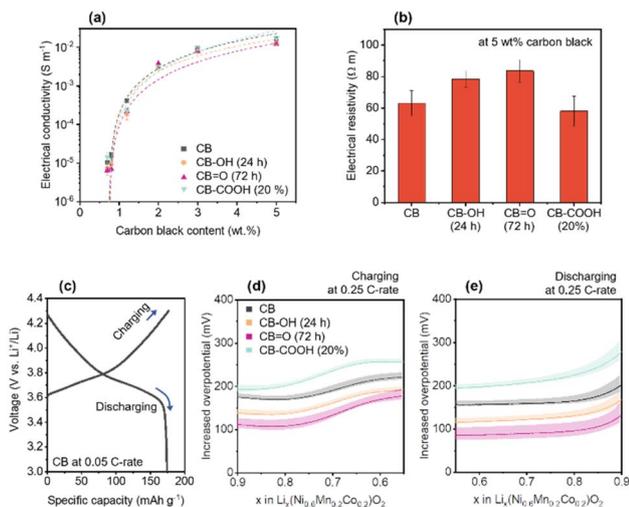
For all samples, switching from a fast (0.25, 0.50, 0.75C) to a slow 0.10 C-rate demonstrated full capacity recovery. This recovery confirms that the performance deterioration of CB–COOH (20%) at high C-rate may originate from electrostatic interactions of Li$^+$ ions with carboxyl groups. Komaba *et al.*[59] have previously shown that Li$^+$ ions can be trapped by electronegative carboxyl groups. Since Li$^+$ trapping is an electrostatic attraction, and reversible, full capacity recover of the CB–COOH (20%) should be expected. A modified CB/polyvinylidene difluoride composite in the cathode, operating between 3 and 4.3 V *vs.* Li$^+$/Li using CV, confirmed this reversibility (Fig. S7†).

Polarization of the electrical double layer is observed up to 300 mV, with no oxidation (anodic) peak. Shuichi *et al.*[60] have observed that oxygen groups in a carbonate medium do not decompose in the range of 1.9–4.9 V *vs.* Li$^+$/Li (symmetric activated carbon electrodes with 1 M triethylmethylammonium (TEMA) tetrafluoroborate (BF$_4$) in propylene carbonate (PC)). Thus, the lack of an oxidation peak precludes any irreversible phase change from occurring.

2.2.2 Resistance and overpotential. To understand this rate improvement for CB–OH (24 h) and C=O (72 h) the resistance to different processes occurring within the cathode were studied. For electrochemical reactions at the LiBs cathode, the resistance experienced by Li$^+$ ions during diffusion occur in 3 locations: (1) inside the NMC ($Z_{Warburg}$ for solid-state diffusion), (2) within the porous structure (R_{ion} for ionic transportation) and (3) on the surface of NMC (R_{CEI} for cathode–electrolyte interphase and R_{ct} for charge-transfer).[61–64] In the case of solid-state diffusion a known deterioration mechanism is the acidic attack of the active material which leads to transition metal dissolution, hydrofluoric acid (HF) production, and associated crystal structure changes.[65] In this work, the oxygen groups are not involved in the deterioration mechanism. The HF can be produced when lithium salt (LiPF$_6$) and water react,[66,67] but the oxygen groups were not decomposed in the 3–4.3 V *vs.* Li$^+$/Li operating range (Fig. S9†). This means that there is no evidence oxygen groups are involved in the acidic attack. In addition, recovery of the capacity at 0.10C after a high current rate (Fig. 2c) showed NMC crystal structure is not influenced by the oxygen groups. Thus, the introduction of oxygen groups on CB does not appears to affect the solid-state diffusion of Li$^+$ ions within the NMC622 active material.

To identify electronic transfer and Li$^+$ ion diffusion within the porous NMC622 cathode structure, out-of-plane electrical conductivity was investigated as a function of CB content (0.7–5 wt%) (Fig. 3a and Note S1, ESI†). The out-of-plane conductivity indirectly demonstrates not only electronic transportation from a current collector to active sites,[20,68,69] but also the passively formed porous structure upon CB dispersion.[19,70] Fig. 3a shows an exponential increase in electrical conductivity with CB content, explained by percolation theory.[71,72] The percolation threshold for each CB in the NMC622 cathode was calculated as follows: CB ($\phi_c = 0.74 \pm 0.05$ wt%); CB–OH (24 h) ($\phi_c = 0.76 \pm 0.09$ wt%); CB=O (72 h) ($\phi_c = 0.74 \pm 0.05$ wt%); and CB–COOH (20%) ($\phi_c = 0.71 \pm 0.07$ wt%). This data clearly shows that there is no significant difference on the distribution of the CBs in the cathode. The electrical resistances of the NMC622 cathode with 5 wt% CB showed C=O (72 h) to have the highest value (CB = 63.2 ± 7.9 Ω m, CB–OH (24 h) = 78.3 ± 5.1 Ω m, CB=O (72 h) = 83.5 ± 7.2 Ω m, and CB–COOH (20%) = 58.0 ± 9.4 Ω m) (Fig. 3b). Despite the highest electrical resistivity, the CB=O (72 h) shows the best electrochemical rate performance in Fig. 2b. Therefore, the enhancement in rate performance does not derive from electrical resistivity of the cathode, rather it may come from chemical and interfacial effects.

To understand how oxygen groups on the surface of CB affect the Li$^+$ ions at the surface of NMC, experiments comparing the potential difference between a pristine CB sample at slow rate of

This journal is © The Royal Society of Chemistry 2024

J. Mater. Chem. A, 2024, **12**, 4884–4892 | **4887**

Fig. 3 (a) Out-of-plane electrical conductivity of NMC622 cathodes with various CB content. The electrical conductivity is fitted with percolation equation (see Note S1, ESI†). (b) Electrical resistivity of the cathodes with 5 wt% CB content. (c) GCD curve for CB at 0.05 C-rate. Calculated overpotentials of the cathodes at 0.25 C-rate versus CB at 0.05 C-rate during (d) charging and (e) discharging. The error bars and bands represent standard deviation.

0.05C (Fig. 3c), and at moderate rate of 0.25C (Fig. 3d and e) was investigated for CB, CB–OH (24 h), CB=O (72 h), and CB–COOH (20%). The potential difference (Fig. 3d and e) is estimated as the voltage difference between NMC622 samples (CB, CB–OH (24 h), CB=O (72 h), and CB–COOH (20%) at 0.25C) with CB (at 0.05C), and thus is termed overpotential.[73] In Fig. 3c, the GCD curve of NMC622 with CB at 0.05C (discharge capacity $\sim$175 mA h g^{-1}) is shown as reference. The x value in Li$_x$(Ni$_{0.6}$Mn$_{0.2}$Co$_{0.2}$)O$_2$ (lithiated NMC622) is calculated based on the theoretical capacity of $\sim$277.4 mA h g^1.

The measured overpotential at 0.25C (Fig. 3d and e) corresponds to the extra voltage that needs to be applied to the system to charge at the faster rate. As the C-rate increases, extra voltage or overpotential is required due to a departure from equilibrium charging/discharging processes, and the subsequent formation of a concentration gradient of Li$^+$ ions in the electrode.[74] In the range of $x = 0.9$ to 0.55 during charging, the NMC is undergoing a phase transition of H1 $\rightarrow$ H2 which corresponds to the expansion of a axis and the contraction of c axis of the NMC lattice simultaneously.[75] As expected, within this $x = 0.9$ to 0.55 range, all NMC cathodes (CB, CB–OH (24 h), CB=O (72 h), and CB–COOH (20%)) cathodes show an increased overpotential at 0.25C compared to a 0.05C CB cathode (Fig. 3d). The CB=O (72 h) cathode demonstrates the lowest overpotential (109 mV at $x = 0.9$) compared to CB 173 mV, CB–OH (24 h) 136 mV, and CB–COOH (20%) 193 mV, indicating that the CB=O (72 h) cathode requires the least energy to charge at faster rates. This trend is also consistent with overpotential on discharging. In Fig. 3e, in the range of $x = 0.55$ to 0.9, the overpotentials are low in order of: CB=O (72 h) 101 mV, CB–OH (24 h) 136 mV, CB 171 mV, and CB–COOH (20%) 235 mV at $x = 0.55$. The CB=O (72 h) reduced the

overpotentials, energy barrier for electrochemical reaction, of 64 and 70 mV compared to pristine CB at 0.25C charging/discharging, respectively.

2.2.3 Electrochemical reactions *via* electrochemical impedance spectroscopy. Electrochemical reactions occurring at the cathode–electrolyte interface can be understood as a series of reactions occurring at different timescales; including cathode–electrolyte interphase formation, charge-transfer reactions, and solid-state diffusion processes.[76] To understanding the observed improvement of CB=O (72 h) compared to CB within the NMC622 cathode (Fig. 2c and d; 3d and e), electrochemical impedance spectroscopy (EIS) was performed (Fig. 4).

The measured EIS spectra were averaged from three cells after normalisation.[73,77] In Fig. 4a, Nyquist plots of CB and CB=O (72 h) cathodes are shown at different applied potentials during charging and discharging. These Nyquist plots comprise of three key regions: (1) a semi-circle at high frequency (100 kHz to 20 Hz) describing interfacial resistance (*e.g.*, cathode–
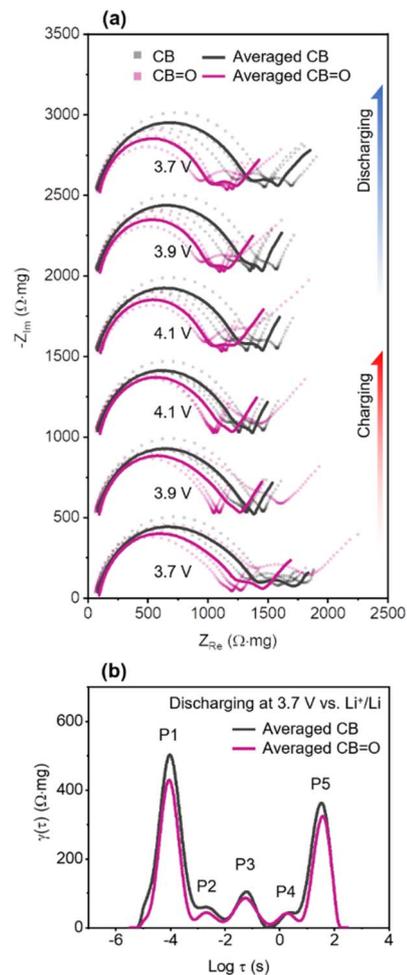
Fig. 4 (a) Nyquist plots of pristine CB and CB=O (72 h) at 3.7, 3.9, and 4.1 V vs. Li$^+$/Li during charging and discharging. The dotted lines denote measurement of individual cells and solid lines are averages. (b) Distribution of relaxation times (DRT) of averaged pristine CB and CB=O (72 h) at 3.7 V vs. Li$^+$/Li discharging.

4888 | J. Mater. Chem. A, 2024, 12, 4884–4892

This journal is © The Royal Society of Chemistry 2024

electrolyte interphase); (2) a relatively small semi-circle at intermediate frequency (20 Hz to 300 mHz) related to charge-transfer resistance; and (3) a Warburg tail at low frequency (<300 mHz) for restricted solid-state diffusion.[78,79] During both charging and discharging processes, CB=O (72 h) NMC622 cathodes exhibited a lower real impedance (Z_{Re}) at high frequencies compared to CB NMC622 cathodes at all studied voltages, denoted by the first semi-circle, indicating lower resistance at cathode–electrolyte interface.

To quantify the impedance of the three different electrochemical processes described above in CB and CB=O (72 h) cathodes, the distribution of relaxation times technique (DRT) was applied to represent discrete impedance data onto continuous time functions (Fig. S10†).[80–84] The DRT curves of CB/NMC622 cathodes and CB=O (72 h)/NMC622 cathodes at 3.7 V vs. Li⁺/Li discharging are illustrated in Fig. 4b, showing 5 distinct polarisation contributions (peaks), labelled P1–P5. The five polarisation contributions can be distinguished by their relaxation time: cathode–electrolyte interphase (P1 at $\log \tau =$ −4.0), charge-transfer reaction (P2–P4 at $\log \tau = $ −2.6, −1.3, and 0.7), and solid-state diffusion (P5 at $\log \tau = $ 1.5).

Firstly, in the case of interfacial resistance at the cathode–electrolyte interphase (CEI), CB/NMC622 cathodes show a higher peak amplitude (494 Ω mg) than CB=O (72 h)/NMC622 cathodes (431 Ω mg). This higher peak amplitude indicates that CB/NMC622 cathode has thicker CEI than the CB=O/NMC622 (72 h) cathode. The CB/NMC622 cathode exhibits inferior surface redox behaviour, in comparison to the CB=O/NMC622 (72 h) cathode, which results in the concentration of Li⁺ ions at the surface of NMC622. The higher concentration of Li⁺ ions lead to an increase local polarisation and current,[85] and subsequently the formation of a thicker CEI.[65] In the case of charge-transfer reaction, CB/NMC622 and CB=O (72 h)/NMC622 cathodes show differences in P2 (59 vs. 45 Ω mg) and P3 (106 vs. 86 Ω mg) with a decreased improvement at slower charge transfer rates at P4 (44 vs. 41 Ω mg). To date, factors contributing to the resistance of each electrochemical reaction are not fully understood.[86] However, improved wetting of the CB=O with the electrolyte (EC/EMC) (Fig. S11†), which may arise from hydrogen bonding interactions between EC/DMC and the carbonyl functional group will increase electrochemically active surface area compared to pristine CB. The improved wetting was demonstrated by dropping 20 µL of 1 M LiPF₆ EC:EMC onto a film of CB and CB=O (72 h) in an argon atmosphere. On CB, the 1 M LiPF₆ EC:EMC showed the distinct formation of a droplet, in contrast it rapidly fully wet the CB=O with no surface droplet visible (Fig. S11†). An increased electrochemically active surface area, particularly creating a higher triple boundary area between NMC622|CB|electrolyte, can enhance the efficiency of a solvated Li⁺ ion migrating into NMC622 by Li accepting an electron. For P5, which represents solid-state diffusion in the DRT curve (Fig. 4b),[87] CB=O/NMC622 was observed to have lower impedance compared to CB/NMC622 (372 vs. 333 Ω mg). This can be explained by the increased wetting ability of the electrolyte on the CB=O/NMC622 and, consequently an increase in the electrochemically active triple boundary area (Fig. 5). This increased
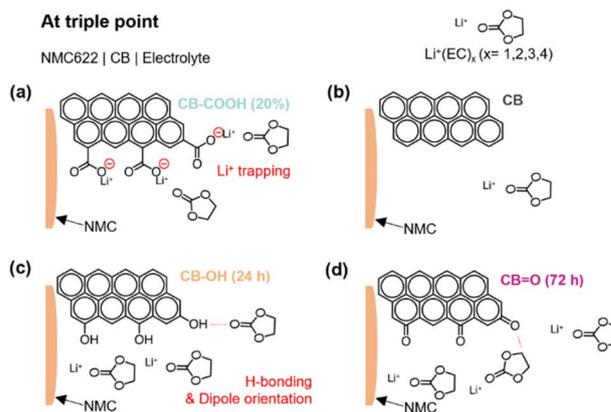

Fig. 5 Schematic model for the role of oxygen-containing groups on the surface of CB at the triple boundary: (a) CB–COOH (20%), (b) CB, (c) CB–OH (24 h), and (d) CB=O (72 h).

electrochemically active boundary area in CB=O/NMC622 means that although the NMC622 is identical in both samples, CB=O/NMC622 has a shorter diffusion length than CB/NMC622. Thus, since the solid-state diffusion coefficient is proportional to the square of diffusion length,[61] the CB=O/NMC622 (with a relatively shorter diffusion length) presents a lower solid-state diffusion impedance (Fig. 4b).

2.3 Demonstration with other cathode materials

To demonstrate the broad applicability of this approach, a comparative rate performance study of CB and CB=O (72 h) as a conductive additive for NMC811, LMO, and NCA cathodes were conducted (Table 2 and Fig. S12†). Compared to CB, the rate performance of all CB=O (72 h) cathodes increased at 0.75C: 62.1 mA h g⁻¹ for NMC622, 71.0 mA h g⁻¹ for NMC811, 6.5 mA h g⁻¹ for LMO and 98.5 mA h g⁻¹ for NCA. Although the dominant cause of rate-limiting differs depending on the cathode materials or electrode structure, CB=O (72 h) can be a general solution to enhance rate capability for LiB cathodes by improving the surface reaction.

2.4 Proposed mechanism of rate enhancement

From the CV, GCD and EIS data, it is clear that by modifying CB with C=O functional groups increases the rate performance of NMC cathodes, while COOH groups demonstrate a negative effect. The improvement observed for CB=O (72 h) arises from a decreased resistance to electrochemical reactions within the cathode active material, including cathode–electrolyte interphase resistance, solid-state diffusion, and charge transfer properties.

The suggested roles of various oxygen functionalities on the surface of CB, for electrochemical reactions at the triple boundary, is illustrated in Fig. 5. In the case of CB–COOH (20%), the negative charge on deprotonated carboxyl groups (COO⁻) can lead to a strong interaction with approaching Li⁺ ions (Fig. 5a). This interaction creates an energy barrier, meaning more energy (i.e., voltage/overpotential) is required to

This journal is © The Royal Society of Chemistry 2024

J. Mater. Chem. A, 2024, **12**, 4884–4892 | **4889**

Table 2 Cathode electrode information including type of active material and carbon black, active material mass loading, and averaged discharge capacity on the rate capability test

Active material	Carbon black	Active material mass [mg cm^{-2}]	Averaged discharge capacity [mA h g^{-1}]				
			0.1C	0.25C	0.5C	0.75C	Δ at 0.75C
NMC622	CB	23.40 ± 0.64	160.8	140.7	98.4	24.4	0.0
NMC622	CB–OH (24 h)	21.20 ± 1.89	162.7	144.9	110.4	65.4	41.0
NMC622	CB=O (72 h)	19.70 ± 0.89	162.9	145.5	119.0	86.5	62.1
NMC622	CB–COOH (20%)	18.99 ± 0.54	162.2	136.1	77.7	16.1	−8.3
NMC811	CB	22.10 ± 0.90	181.3	152.5	111.1	65.2	0.0
NMC811	CB=O (72 h)	20.67 ± 1.88	193.6	180.7	159.9	136.2	71.0
LMO	CB	18.99 ± 0.33	116.8	111.7	103.0	91.9	0.0
LMO	CB=O (72 h)	20.42 ± 1.03	117.3	113.2	106.5	98.4	6.5
NCA	CB	22.24 ± 0.12	165.1	123.9	45.5	0.0	0.0
NCA	CB=O (72 h)	21.00 ± 0.42	153.8	140.2	120.8	98.5	98.5

enable further Li$^+$ ion motion (*via* diffusion, intercalation or deintercalation).

In contrast, CB–OH (24 h) (Fig. 5c) and CB=O (72 h) (Fig. 5d) showed an increased rate performance compared to pristine CB due to the increased electrolyte wettability (Fig. S11†) arising from dipole interactions between the hydrogen atom (*e.g.*, CB=O⋯ in ethylene carbonate) and the oxygen atom (*e.g.*, CB–OH⋯O in ethylene carbonate) of the carbonate solvent. Considering that Li$^+$ ions are transported through the solvent phase, through an interaction with the oxygen group in the carbonate solvent, the proposed dipole attraction may limit Li$^+$ ion transportation by acting as a competing mechanism.

3. Conclusions

Carbon black is a critical, yet understudied, component of the LiB cathode. Here, mild oxidation processes are used to tune the oxygen-containing functional groups on the surface of carbon blacks, which results in a marked improvement in NCM622 cathode rate capability (from 24.4 mA h g^{-1} to 86.5 mA h g^{-1} at 0.75C). Introducing carbonyl groups (C=O) or hydroxyl groups (C–OH) onto the surface of carbon black resulted in a dramatic improvement in rate performance, while the formation of carboxyl groups (COOH) resulted in significantly lower cathode rate capability. This concept was extended, with C=O (72 h) functionalised carbon blacks showing improved rate performance across commonly used cathode active materials, including NMC811, LMO, and NCA. This work provides a simple pathway for enhancing the rate capability of LiB cathodes in carbonate solvents.

Conflicts of interest

There are no conflicts to declare.

Acknowledgements

Notes and references

1 J. B. Goodenough and K.-S. Park, *J. Am. Chem. Soc.*, 2013, **135**, 1167–1176.
2 J. Liu, Z. Bao, Y. Cui, E. J. Dufek, J. B. Goodenough, P. Khalifah, Q. Li, B. Y. Liaw, P. Liu, A. Manthiram, Y. S. Meng, V. R. Subramanian, M. F. Toney, V. V. Viswanathan, M. S. Whittingham, J. Xiao, W. Xu, J. Yang, X.-Q. Yang and J.-G. Zhang, *Nat. Energy*, 2019, **4**, 180–186.
3 W. Cao, B. C. Mecrow, G. J. Atkinson, J. W. Bennett and D. J. Atkinson, *IEEE Trans. Ind. Electron.*, 2011, **59**, 3523–3531.
4 J. Rosero, J. Ortega, E. Aldabas and L. Romeral, *IEEE Aero. Electron. Syst. Mag.*, 2007, **22**, 3–9.
5 M. Gutsch and J. Leker, *J. Energy Storage*, 2022, **52**, 105030.
6 D. Larcher and J. M. Tarascon, *Nat. Chem.*, 2015, **7**, 19–29.
7 A. Kwade, W. Haselrieder, R. Leithoff, A. Modlinger, F. Dietrich and K. Droeder, *Nat. Energy*, 2018, **3**, 290–300.
8 A. Manthiram, *Nat. Commun.*, 2020, **11**, 1550.
9 Z. Chen, W. Zhang and Z. Yang, *Nanotechnology*, 2020, **31**, 012001.
10 R. Amin and Y.-M. Chiang, *J. Electrochem. Soc.*, 2016, **163**, A1512.
11 L.-X. Yuan, Z.-H. Wang, W.-X. Zhang, X.-L. Hu, J.-T. Chen, Y.-H. Huang and J. B. Goodenough, *Energy Environ. Sci.*, 2011, **4**, 269–284.
12 X. Zhu, T. U. Schulli, X. Yang, T. Lin, Y. Hu, N. Cheng, H. Fujii, K. Ozawa, B. Cowie, Q. Gu, S. Zhou, Z. Cheng, Y. Du and L. Wang, *Nat. Commun.*, 2022, **13**, 1565.
13 X. Han, Y. Gong, K. K. Fu, X. He, G. T. Hitz, J. Dai, A. Pearse, B. Liu, H. Wang, G. Rubloff, Y. Mo, V. Thangadurai, E. D. Wachsman and L. Hu, *Nat. Mater.*, 2017, **16**, 572–579.

14 X. Yu and A. Manthiram, *Energy Environ. Sci.*, 2018, **11**, 527–543.

15 W. Li, A. Dolocan, P. Oh, H. Celio, S. Park, J. Cho and A. Manthiram, *Nat. Commun.*, 2017, **8**, 14589.

16 S. Choudhury, R. Mangal, A. Agrawal and L. A. Archer, *Nat. Commun.*, 2015, **6**, 10101.

17 T. Marks, S. Trussler, A. Smith, D. Xiong and J. Dahn, *J. Electrochem. Soc.*, 2010, **158**, A51.

18 W. Bauer and D. Nötzel, *Ceram. Int.*, 2014, **40**, 4591–4598.

19 Y. Itou, N. Ogihara and S. Kawauchi, *J. Phys. Chem. C*, 2020, **124**, 5559–5564.

20 S.-H. Park, P. J. King, R. Tian, C. S. Boland, J. Coelho, C. Zhang, P. McBean, N. McEvoy, M. P. Kremer, D. Daly, J. N. Coleman and V. Nicolosi, *Nat. Energy*, 2019, **4**, 560–567.

21 M. Jerigova, M. Odziomek and N. Lopez-Salas, *ACS Omega*, 2022, **7**, 11544–11554.

22 J. Zhang, H. Zou, Q. Qing, Y. Yang, Q. Li, Z. Liu, X. Guo and Z. Du, *J. Phys. Chem. B*, 2003, **107**, 3712–3718.

23 Y.-C. Chiang, W.-H. Lin and Y.-C. Chang, *Appl. Surf. Sci.*, 2011, **257**, 2401–2410.

24 T. A. Saleh, *Appl. Surf. Sci.*, 2011, **257**, 7746–7751.

25 T. J. Aitchison, M. Ginic-Markovic, J. G. Matisons, G. P. Simon and P. M. Fredericks, *J. Phys. Chem. C*, 2007, **111**, 2440–2446.

26 A. Rasheed, J. Y. Howe, M. D. Dadmun and P. F. Britt, *Carbon*, 2007, **45**, 1072–1080.

27 V. Datsyuk, M. Kalyva, K. Papagelis, J. Parthenios, D. Tasis, A. Siokou, I. Kallitsis and C. Galiotis, *Carbon*, 2008, **46**, 833–840.

28 K. A. Wepasnick, B. A. Smith, K. E. Schrote, H. K. Wilson, S. R. Diegelmann and D. H. Fairbrother, *Carbon*, 2011, **49**, 24–36.

29 D. Pan, S. Wang, B. Zhao, M. Wu, H. Zhang, Y. Wang and Z. Jiao, *Chem. Mater.*, 2009, **21**, 3136–3142.

30 E. Lee and K. A. Persson, *Nano Lett.*, 2012, **12**, 4624–4628.

31 Y. Okamoto, *J. Phys. Chem. C*, 2016, **120**, 14009–14014.

32 K. Nishidate and M. Hasegawa, *Phys. Rev. B: Condens. Matter Mater. Phys.*, 2005, **71**, 245418.

33 V. Meunier, J. Kephart, C. Roland and J. Bernholc, *Phys. Rev. Lett.*, 2002, **88**, 075506.

34 C. B. Robledo, J. E. Thomas, G. Luque, E. P. M. Leiva, O. Cámara, D. Barraco and A. Visintin, *Electrochim. Acta*, 2014, **140**, 160–167.

35 T.-H. Kim, E. K. Jeon, Y. Ko, B. Y. Jang, B.-S. Kim and H.-K. Song, *J. Mater. Chem. A*, 2014, **2**, 7600–7605.

36 M. J. Matthews, M. A. Pimenta, G. Dresselhaus, M. Dresselhaus and M. Endo, *Phys. Rev. B: Condens. Matter Mater. Phys.*, 1999, **59**, R6585.

37 T. Jawhari, A. Roid and J. Casado, *Carbon*, 1995, **33**, 1561–1565.

38 S. Eigler, C. Dotzer and A. Hirsch, *Carbon*, 2012, **50**, 3666–3673.

39 Y. Peng and H. Liu, *Ind. Eng. Chem. Res.*, 2006, **45**, 6483–6488.

40 J. Vicente-Santiago, J. Cornejo-Jacob, D. Valdez-Perez, J. Ruiz-Garcia and R. A. Guirado-Lopez, *Phys. Chem. Chem. Phys.*, 2019, **21**, 24077–24091.

41 S. Wang, Z.-H. Chen, W.-J. Ma and Q.-S. Ma, *Ceram. Int.*, 2006, **32**, 291–295.

42 E. Desimoni, G. Casella, A. Morone and A. M. Salvi, *Surf. Interface Anal.*, 1990, **15**, 627–634.

43 J. J. Ternero-Hidalgo, J. M. Rosas, J. Palomo, M. J. Valero-Romero, J. Rodríguez-Mirasol and T. Cordero, *Carbon*, 2016, **101**, 409–419.

44 J.-H. Kim, S. Y. Hwang, J. E. Park, G. B. Lee, H. Kim, S. Kim and B. U. Hong, *Carbon Lett.*, 2019, **29**, 281–287.

45 G. Gao, M. Pan and C. D. Vecitis, *J. Mater. Chem. A*, 2015, **3**, 7575–7582.

46 M. Acik, G. Lee, C. Mattevi, M. Chhowalla, K. Cho and Y. Chabal, *Nat. Mater.*, 2010, **9**, 840–845.

47 C. D. Quilty, G. P. Wheeler, L. Wang, A. H. McCarthy, S. Yan, K. R. Tallman, M. R. Dunkin, X. Tong, S. Ehrlich and L. Ma, *ACS Appl. Mater. Interfaces*, 2021, **13**, 50920–50935.

48 S. Li, T. Zhao, K. Wang, C. Sun, W. Jia, M. Zhang, H. Wang, A. Shao and Y. Ma, *Adv. Funct. Mater.*, 2022, **32**, 2203010.

49 Y. Bai, R. Essehli, C. J. Jafta, K. M. Livingston and I. Belharouak, *ACS Sustainable Chem. Eng.*, 2021, **9**, 6048–6055.

50 T. Brezesinski, J. Wang, S. H. Tolbert and B. Dunn, *Nat. Mater.*, 2010, **9**, 146–151.

51 A. J. Bard, L. R. Faulkner and H. S. White, *Electrochemical Methods: Fundamentals and Applications*, John Wiley & Sons, 2022.

52 G. Lai, P. Ruan, X. Hu, B. Lu, S. Liang, Y. Tang and J. Zhou, *J. Mater. Chem. A*, 2023, **11**, 15211–15218.

53 X. Yang and A. L. Rogach, *Adv. Energy Mater.*, 2019, **9**, 1900747.

54 T. Kim, W. Choi, H.-C. Shin, J.-Y. Choi, J. M. Kim, M.-S. Park and W.-S. Yoon, *J. Electrochem. Sci. Technol.*, 2020, **11**, 14–25.

55 M. Evertz, F. Horsthemke, J. Kasnatscheew, M. Börner, M. Winter and S. Nowak, *J. Power Sources*, 2016, **329**, 364–371.

56 I. Buchberger, S. Seidlmayer, A. Pokharel, M. Piana, J. Hattendorff, P. Kudejova, R. Gilles and H. A. Gasteiger, *J. Electrochem. Soc.*, 2015, **162**, A2737.

57 R. Jung, F. Linsenmann, R. Thomas, J. Wandt, S. Solchenbach, F. Maglia, C. Stinner, M. Tromp and H. A. Gasteiger, *J. Electrochem. Soc.*, 2019, **166**, A378.

58 P. Zhu, V. Trouillet, S. Heißler and W. Pfleging, *J. Energy Storage*, 2023, **66**, 107401.

59 S. Komaba, N. Yabuuchi, T. Ozeki, K. Okushi, H. Yui, K. Konno, Y. Katayama and T. Miura, *J. Power Sources*, 2010, **195**, 6069–6074.

60 S. Ishimoto, Y. Asakawa, M. Shinya and K. Naoi, *J. Electrochem. Soc.*, 2009, **156**, A563.

61 C. Zhu, R. E. Usiskin, Y. Yu and J. Maier, *Science*, 2017, **358**, 1400.

62 H. Gao, Q. Wu, Y. Hu, J. P. Zheng, K. Amine and Z. Chen, *J. Phys. Chem. Lett.*, 2018, **9**, 5100–5104.

63 N. Ogihara, S. Kawauchi, C. Okuda, Y. Itou, Y. Takeuchi and Y. Ukyo, *J. Electrochem. Soc.*, 2012, **159**, A1034.

64 W. Choi, H.-C. Shin, J. M. Kim, J.-Y. Choi and W.-S. Yoon, *J. Electrochem. Sci. Technol.*, 2020, **11**, 1–13.

This journal is © The Royal Society of Chemistry 2024

J. Mater. Chem. A, 2024, **12**, 4884–4892 | **4891**

65 K. Guo, S. Qi, H. Wang, J. Huang, M. Wu, Y. Yang, X. Li, Y. Ren and J. Ma, *Small Sci.*, 2022, **2**, 2100107.

66 Y. Tesfamhret, R. Younesi and E. J. Berg, *J. Electrochem. Soc.*, 2022, **169**, 010530.

67 Y. Tesfamhret, H. Liu, Z. Chai, E. Berg and R. Younesi, *ChemElectroChem*, 2021, **8**, 1516–1523.

68 R. Tian, N. Alcala, S. J. K. O'Neill, D. V. Horvath, J. Coelho, A. J. Griffin, Y. Zhang, V. Nicolosi, C. O'Dwyer and J. N. Coleman, *ACS Appl. Energy Mater.*, 2020, **3**, 2966–2974.

69 X. Zhang, Z. Ju, Y. Zhu, K. J. Takeuchi, E. S. Takeuchi, A. C. Marschilok and G. Yu, *Adv. Energy Mater.*, 2020, **11**, 2000808.

70 H. Bockholt, W. Haselrieder and A. Kwade, *Powder Technol.*, 2016, **297**, 266–274.

71 Z. Ju, X. Zhang, S. T. King, C. D. Quilty, Y. Zhu, K. J. Takeuchi, E. S. Takeuchi, D. C. Bock, L. Wang, A. C. Marschilok and G. Yu, *Appl. Phys. Rev.*, 2020, **7**, 041405.

72 D. Park and K. Kim, *J. Appl. Phys.*, 2021, **130**, 204101.

73 J. J. Kuo, S. D. Kang and W. C. Chueh, *Adv. Energy Mater.*, 2022, **12**, 2201114.

74 S. Müller, J. Eller, M. Ebner, C. Burns, J. Dahn and V. Wood, *J. Electrochem. Soc.*, 2018, **165**, A339.

75 C. D. Quilty, D. C. Bock, S. Yan, K. J. Takeuchi, E. S. Takeuchi and A. C. Marschilok, *J. Phys. Chem. C*, 2020, **124**, 8119–8128.

76 S. Wang, J. Zhang, O. Gharbi, V. Vivier, M. Gao and M. E. Orazem, *Nat. Rev. Methods Primers*, 2021, **1**, 41.

77 M. A. Kamenskii, S. N. Eliseeva, E. G. Tolstopjatova, A. I. Volkov, D. V. Zhuzhelskii and V. V. Kondratiev, *Electrochim. Acta*, 2019, **326**, 134969.

78 G. Assat, D. Foix, C. Delacourt, A. Iadecola, R. Dedryvere and J. M. Tarascon, *Nat. Commun.*, 2017, **8**, 2219.

79 L. Wang, J. Zhao, X. He, J. Gao, J. Li, C. Wan and C. Jiang, *Int. J. Electrochem. Sci.*, 2012, **7**, 345–353.

80 Q. Meyer, S. Liu, Y. Li and C. Zhao, *J. Power Sources*, 2022, **533**, 231058.

81 R. Soni, J. B. Robinson, P. R. Shearing, D. J. L. Brett, A. J. E. Rettie and T. S. Miller, *Energy Storage Mater.*, 2022, **51**, 97–107.

82 H. Jia, L. Zou, P. Gao, X. Cao, W. Zhao, Y. He, M. H. Engelhard, S. D. Burton, H. Wang, X. Ren, Q. Li, R. Yi, X. Zhang, C. Wang, Z. Xu, X. Li, J. G. Zhang and W. Xu, *Adv. Energy Mater.*, 2019, **9**, 1900784.

83 F. Ciucci and C. Chen, *Electrochim. Acta*, 2015, **167**, 439–454.

84 T. H. Wan, M. Saccoccio, C. Chen and F. Ciucci, *Electrochim. Acta*, 2015, **184**, 483–499.

85 A. Jana, S. I. Woo, K. S. N. Vikrant and R. E. García, *Energy Environ. Sci.*, 2019, **12**, 3595–3607.

86 R. He, Y. He, W. Xie, B. Guo and S. Yang, *Energy*, 2023, **263**, 125972.

87 X. Zhu, L. Cheng, H. Yu, F. Xu, W. Wei and L.-Z. Fan, *J. Materiomics*, 2022, **8**, 649.

4892 | *J. Mater. Chem. A*, 2024, **12**, 4884–4892

This journal is © The Royal Society of Chemistry 2024